metals

MDPI

Article

Fast Gold Recovery from Aqueous Solutions and Assessment of Antimicrobial Activities of Novel Gold Composite

Tamara Tadić [1], Bojana Marković [1], Zorica Vuković [1], Plamen Stefanov [2], Danijela Maksin [3], Aleksandra Nastasović [1] and Antonije Onjia [4,*]

[1] Institute of Chemistry, Technology and Metallurgy, University of Belgrade, Njegoševa 12, 11000 Belgrade, Serbia; tamara.tadic@ihtm.bg.ac.rs (T.T.); bojana.markovic@ihtm.bg.ac.rs (B.M.); zvukovic@nanosys.ihtm.bg.ac.rs (Z.V.); aleksandra.nastasovic@ihtm.bg.ac.rs (A.N.)
[2] Institute of General and Inorganic Chemistry, Bulgarian Academy of Sciences, Acad. Georgi Bonchev Str., bld. 11, 1113 Sofia, Bulgaria; stefanov@svr.igic.bas.bg
[3] Vinča Institute of Nuclear Sciences, University of Belgrade, 11000 Belgrade, Serbia; dmaksin@vin.bg.ac.rs
[4] Faculty of Technology and Metallurgy, University of Belgrade, Karnegijeva 4, 11000 Belgrade, Serbia
* Correspondence: onjia@tmf.bg.ac.rs

Abstract: A novel porous gold polymer composite was prepared by the functionalization of a glycidyl methacrylate-based copolymer (pGME) with ethylene diamine (pGME-en), and activation by gold (pGME-en/Au), in a simple batch adsorption procedure in an acid solution, at room temperature. Detailed characterization of the pGME-en before and after activation was performed. The main focuses of this research were the design of a method that can enable the recovery of gold and the reuse of this multipurpose sorbent as an antimicrobial agent. Fourier transform infrared spectroscopy (FTIR) and X-ray photoelectron spectroscopy (XPS) analysis pointed out amine groups as the primary binding sites for Au activation, while hydroxyl groups also contributed to the chelation reaction. pGME-en exhibited fast gold adsorption with an adsorption half-time of 5 min and an equilibrium time of 30 min. The maximal adsorption capacity was about 187 mg/g. The analysis of sorption experimental data with a non-linear surface reaction and diffusion-based kinetic models revealed the pseudo-second-order and Avrami model as the best fit, with unambiguous control by liquid film and intra-particle diffusion. The biological activity studies against *Staphylococcus aureus*, *Listeria monocytogenes*, *Escherichia coli*, and *Candida albicans* revealed moderate activity of pGME-en/Au against different bacterial and fungal species. pGME-en/Au was stable in a saline solution, with a release of approximately 2.3 mg/g after 24 h.

Keywords: glycidyl methacrylate; adsorption; Au; antimicrobial activity; XPS

Citation: Tadić, T.; Marković, B.; Vuković, Z.; Stefanov, P.; Maksin, D.; Nastasović, A.; Onjia, A. Fast Gold Recovery from Aqueous Solutions and Assessment of Antimicrobial Activities of Novel Gold Composite. *Metals* **2023**, *13*, 1864. https://doi.org/10.3390/met13111864

Academic Editors: Bernd Friedrich and Alexander Birich

Received: 11 October 2023
Revised: 27 October 2023
Accepted: 31 October 2023
Published: 9 November 2023

1. Introduction

Gold nanoparticles (AuNPs), due to their outstanding characteristics, such as low contact electrical resistance, excellent electrical conductivity, and exceptional corrosion resistance, have been widely used in optoelectronics, electrochemistry, catalysis, biosensors, antibacterial applications, etc. [1–3]. However, being one of the rarest elements on earth, the mining of gold (Au) is extremely costly. In addition, the U.S. Geological Survey's 2019 annual report revealed the expectation that Earth's commercially mineable gold reserves will be exhausted within the next 15 years. Recent studies imply that Au recovery from electronic waste (e-waste), "urban mining", as well as from seawater, incinerated sludge, and waster effluents, where Au is present in trace quantities, is becoming more cost-effective than the traditional mining of ores [4]. E-waste generated by discarded electrical and electronic equipment (smartphones, computers, displays, etc.) contains precious metals (gold, silver, and palladium), as well as toxic heavy metals, particulate matter, and volatile and semi-volatile organic compounds [5]. Up till now, large quantities of e-waste were disposed in developing regions such as West Africa. It is the most rapidly

increasing form of solid waste, with a worldwide generated amount of 60 million metric tons in 2022, and is projected to reach 74.7 metric tons by 2030 [6]. Hence, in order to meet the demands of sustainable economic development and a circular economy, there is an increasing need for innovative and efficient materials and technologies for metal recovery from different effluents. Various methods, such as hydrometallurgy, pyrometallurgy, leaching, and combinations of these techniques, have been used for metal recovery. Also, flotation is another useful methods to level up metals recovery [7,8].

Gold recovery can be carried out by solvent extraction, membrane separation, chemical precipitation, ion exchange, adsorption, etc. [9]. The adsorption method is simple, eco-friendly, has low operating costs, and is characterized by a high efficiency and reusability of the adsorbent in several adsorption/desorption cycles. In recent years, the attention of researchers to porous materials, based on chelating polymer ligands and investigating their potential use in technologies for precious metal recovery, reuse, and recycling, has increased significantly. Chelating polymer incorporates a polymer support and chemically immobilized ligands, usually consisting of mono-, bi-, or polydentate groups with nitrogen and/or charged or neutral oxygen donor groups [10]. Chelating groups may be covalently bound to a polymer as pendant groups or incorporated into the repeating units of the polymer backbone by the polymerization of a suitable monomer containing the required chelating group. The presence of porous channels, their large surface area, and their unique chemical characteristics have led to the numerous potential applications of these porous materials [11–17]. Among them, the chelating polymer ligands based on glycidyl methacrylate (GMA) are very attractive, due to the presence of oxirane rings that can easily be transformed into various functional groups [18]. These materials have found applications in very diverse areas such as drug delivery [19], support for enzymes [20], and wastewater treatment [21], as well as catalysis [22]. As a result of extensive research, Jovanović et al. developed GMA-based polymeric sorbents with adjustable porosity parameters by varying the type and the amount of aliphatic alcohol and crosslinking monomer in the reaction mixture [23]. A plethora of amino-functionalized porous polymers and composites were used as heavy and precious metal sorbents, with the possibility to coordinate gold and platinum metals or bind them as chloro complexes as basic ion exchangers, depending on pH [24–29].

Chelating GMA-based polymer ligands are considered to be an efficient agent for preparing polymer–metal chelates with desired properties and applications. The affinity or strength of the metal–ligand interaction is influenced by the functionality of the chelating group, density of chelating groups in the polymer, crosslinking density (for copolymers), oxidation state and metal electronic configuration, stereochemistry, steric constraints, and electrostatic interactions [30].

Growing bacterial resistance is a serious problem that requires a quick solution. The antibacterial activity of silver, gold, copper, titanium, zinc oxide, and magnesium oxide nanoparticles (NPs) is well known. Metal NPs can be immobilized in a polymer matrix by in situ synthesis of NPs within the polymer as a reaction medium, or by ex situ synthesis, by adding previously prepared NPs into the polymer matrix as a dispersion medium [31]. To the best of our knowledge, there are few reports investigating the antimicrobial activity of GMA-supported NPs [32–34].

The design and development of antibacterial polymer-supported materials, which can be easily functionalized, could improve their antimicrobial properties due to the synergistic effect between NPs and the polymer matrix, and solve the NP aggregation problem. The main highlight of this research was the recovery of gold, using a novel porous amino-functionalized GMA-based sorbent, and so, the prepared gold polymer composite was examined for possible antibacterial and antifungal activities.

2. Materials and Methods

2.1. Reagents

GMA, cyclohexanol, dodecanol, 2,2′-azobisisobutyronitrile (AIBN), and gold(III) chloride solution ($HAuCl_4$) were purchased from Merck (Darmstadt, Germany). EGDMA and ethylene diamine were obtained from Sigma-Aldrich (St. Louis, MI, USA). Poly(N-vinyl pyrrolidone) (PVP, Kollidone 90) was purchased from BASF SE (Ludwigshafen, Germany). Hydrochloric acid (HCl, 37 *w*/*w*%) and nitric acid (HNO_3, 65 *w*/*w*%) were purchased from Honeywell International, Inc. (Charlotte, NC, USA). All the chemicals were of analytical grade and used without further processing.

2.2. Preparation of Polymeric Adsorbent

A porous crosslinked pGME copolymer was synthesized by the suspension copolymerization of GMA and EGDMA in the presence of a mixture of cyclohexanol and dodecanol as an inert component, AIBN as an initiator, and PVP as a suspension stabilizer [35]. The obtained copolymer was sieved to control the beads' size. Then, 5 g pGME (diameter range from 150 to 500 nm) was modified with a tenfold excess of ethylene diamine in toluene at 70 °C for 7 h. The amino-functionalized copolymer was finally purified by Soxhlet extraction with ethanol, dried in a vacuum oven at 50 °C, and labeled as pGME-en.

2.3. Adsorption Experiments

The working solution of gold was prepared by dissolving $HAuCl_4$ in aqua regia. The adsorption experiment was carried out by contacting 0.5 g of pGME-en with 40 mL $HAuCl_4$ solution, at a pH of 1.5 at room temperature. The aliquots (1 mL) were withdrawn at 1, 5, 30, 60, 90, 120, and 180 min from the beginning of the adsorption process and diluted with deionized water (Milli-Q Millipore, conductivity 18 MW/cm). Each sample aliquot was filtered through a 0.22 µm filter and the gold concentration was determined by inductively coupled plasma optical emission spectrometry (ICP-OES, Model ICP\6500 Perkin Elmer, Waltham, MA, USA). The sorption capacity, Q_t (mg/g), was calculated using Equation (1):

$$Q_t = \frac{(C_i - C_t)\,V}{m} \quad (1)$$

where C_i (mg/L) and C_t (mg/L) are the concentrations of Au ions in the initial solution and in the aqueous phase at time t, respectively, V (L) s the volume of the aqueous phase, and m (g) is the amount of pGME-en adsorbent. All the adsorption experiments were performed in triplicate, and, for further data processing, the average values were used. The pGME-en copolymer with immobilized gold, a gold polymer composite, was rinsed with distilled water and ethanol several times, dried at 50 °C for 24 h under vacuum, and named pGME-en/Au.

2.4. Methods of Characterization

The morphology of the copolymer before and after gold adsorption was investigated by SEM (JEOL JSM-6460 LV, JEOL Ltd., Tokyo, Japan) at desired magnifications. Prior to SEM analysis, the pGME-en was coated with a thin layer of gold to minimize charging. An EDS (Oxford Instruments XMax SDD 20 mm^2, Oxford Instruments Nanoanalysis, High Wycombe, UK) coupled to a JEOL JSM-6460 LV SEM was used to provide elemental identification. The EDS analysis enabled the investigation of the elements' distribution at a depth of 100–1000 nm from the surface. The porosity of all samples was determined by a high-pressure mercury intrusion porosimeter (Carlo Erba 2000, software Milestone 200, Washington, DC, USA). Sample preparation was performed at room temperature and at a pressure of 0.5 kPa. The porosity parameters, i.e., the values of specific pore volume, *Vs*, and pore diameter, which corresponds to half of pore volume, $D_{V/2}$, were read from the pore size distribution curves determined by mercury porosimetry, while the specific surface area, $S_{s,Hg}$, was calculated as the sum of incremental specific surface area from the pore size distribution curves. The thermal stability of the samples was investigated using

a TG/DSC 111 (SETARAM S.A. France, Caluire-et-Cuire, France). The experiments were carried out in an inert atmosphere (30 mL/min) and heated at 10 °C/min up to 450 °C. FTIR analysis was performed in ATR (attenuated total reflection) mode using a Nicolet 380 spectrometer (Thermo Scientific, Waltham, MA, USA) with a Smart OrbitTM ATR attachment (wavenumber range 400–4000 cm^{-1}, resolution 2 cm^{-1}). The surface chemical analysis by XPS was acquired using a VG ESCALAB II instrument (VG Scientific, Waltham, MA, USA) with a non-monochromatized Al K_α line ($h\nu$ of 1486.6 eV, resolution of 1 eV, angle of 45° and base pressure of 1×10^{-8} Pa). The survey scan range was run in the binding energy range of 0–1200 eV in FAT 40 mode, with a pass energy of 80 eV, an energy step of 0.5 eV, and a dwell time of 0.2. High-resolution spectra were taken in FAT 20 mode, with an energy step of 0.1 eV and a dwell time of 1 s.

The experiment investigating Au ions release was carried out in static conditions, by adding 0.5 g pGME-en copolymer with immobilized Au ions into 50 mL of physiological saline solution (9 g/L NaCl) at room temperature. The concentration of the released Au ions was measured in duplicate.

2.5. Antibacterial Activity Assay

The agar plate method was used to assess the antimicrobial activity of pGME-en/Au. The material suspension (200 mg/mL) was made and 50 µL of the suspension was added to the 5 mm-wide well in the agar plate. A nutrient agar medium (DSMZ 1) was used, containing the following ingredients (g/L): peptone (5.0 g), meat extract (3.0 g), agar (20.0 g), distilled water (1.0 L); a pH of 7.0 was used. Plates were inoculated with the Gram-positive strains *S. aureus* ATCC 25923 and *L. monocytogenes* NCTC 11994, the Gram-negative strain *E. coli* NCTC 2001, and the fungal strain *C. albicans* ATCC 10231. The inoculums were 5 × 105 colony-forming units, cfu/mL, for bacteria and 1 × 105 cfu/mL, for *Candida* species. Plates were incubated for 24 h at 37 °C, and the zone of clearance was measured. The methodology flowchart is shown in Figure 1.

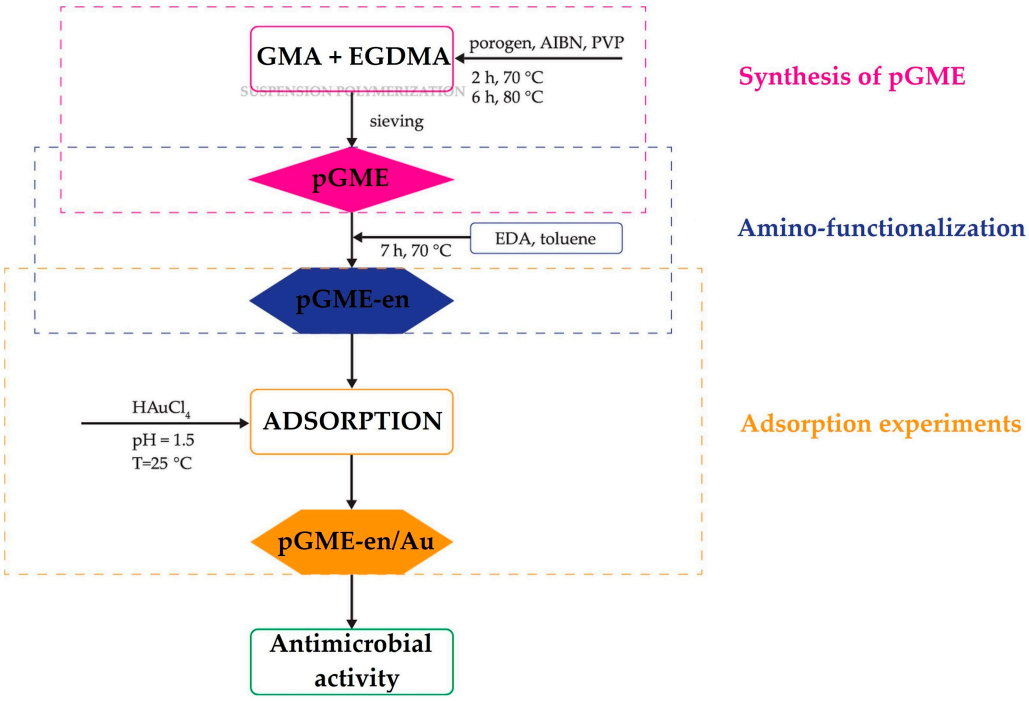

Figure 1. Methodology flowchart.

3. Results and Discussion

3.1. Adsorbent Characterization

The surface morphology of pGME and pGME-en was examined using SEM analysis and is presented in Figure 2a–d. As can be seen, pGME and PGME-en particles are spherical in shape, with a porous surface texture. Qualitative SEM-EDS analysis (Figure 2e) confirmed the presence of all expected elements (C, O, and N). The presence of N peaks (19.4 *w*/*w*%) corroborates the successful amino modification of pGME.

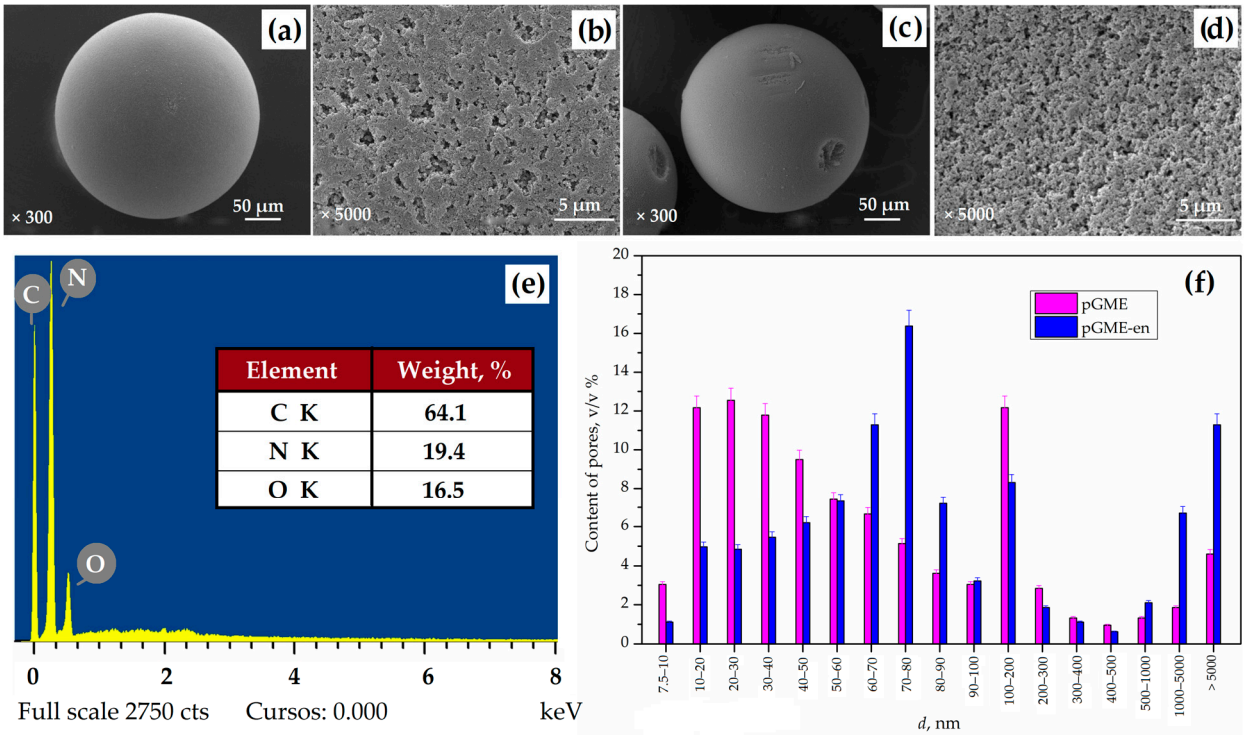

Figure 2. SEM microphotographs of pGME beads at a magnification of (**a**) 300 ×, (**b**) 5000 ×; pGME-en beads at a magnification of (**c**) 300 ×, (**d**) 5000 ×; (**e**) EDS spectra of pGME-en; and (**f**) the pore size distribution diagrams for pGME and pGME-en.

Figure 2f shows pore size distribution diagrams for pGME and pGME-en. A significant shift in the pore size distributions toward larger pore sizes for the amino-functionalized sample, in comparison to the initial one, can be observed. For pGME, the predominant pore range was 10–50 nm (47.7 *v*/*v*%) and, for pGME-en, it shifted to 50–100 nm (46.5 *v*/*v*%). The values of relevant porosity parameters for both samples are given in Table 1.

Table 1. Porosity parameters of initial pGME and amino-functionalized pGME-en.

Sample	$S_{S,Hg}$, m^2/g	V_S, cm^3/g	$d_{V/2}$, nm
pGME	58	0.53	51
pGME-en	84	0.80	78

The results show that amino-functionalization causes the alteration of porosity parameters of pGME. The introduction of amino groups to pGME increases the pore volume (almost 1.5 times) and pore diameter, leading to an increase in the specific surface area of 45%. Namely, the sample of pGME-en has the higher specific volume due to a high amount of macropores (~77 *v*/*v*%), which contribute most to the increase in pore volume, especially pores > 1000 nm (17.5 *v*/*v*%), while the pGME has a lower amount of these pores.

Figure 3a shows the TGA weight losses of pGME and pGME-en versus temperature. As can be seen, the degradation of both samples takes place in three stages. The pGME

demonstrated that the first weight loss stage is in the range between 172 and 218 °C, the second stage is in the range between 218 °C and 361 °C, and the third weight loss is between 361 °C and 450 °C. As for pGME-en, the first stage took place between 192 °C and 252 °C, the second remarkable second weight loss was in the range between 252 and 343 °C, and the last stage was between 343 and 450 °C. The main degradation mechanism of the investigated samples was the depolymerization of monomers and oligomers, initiated by the scission of weak linkages (i.e., H–H bonds, double bonds in backbone pendant groups, and random chain scission), ester decomposition, and the elimination of the amine groups that simultaneously occur [29,36]. Also, the relative thermal stabilities of the samples were assessed by comparing the initial temperature of degradation (T_i) and the temperature at 50% weight loss ($T_{50\%}$). The values of T_i and $T_{50\%}$ of pGME-en (192 °C and 371 °C) were higher than that of pGME (172 °C and 313 °C), suggesting an increase in thermal stability.

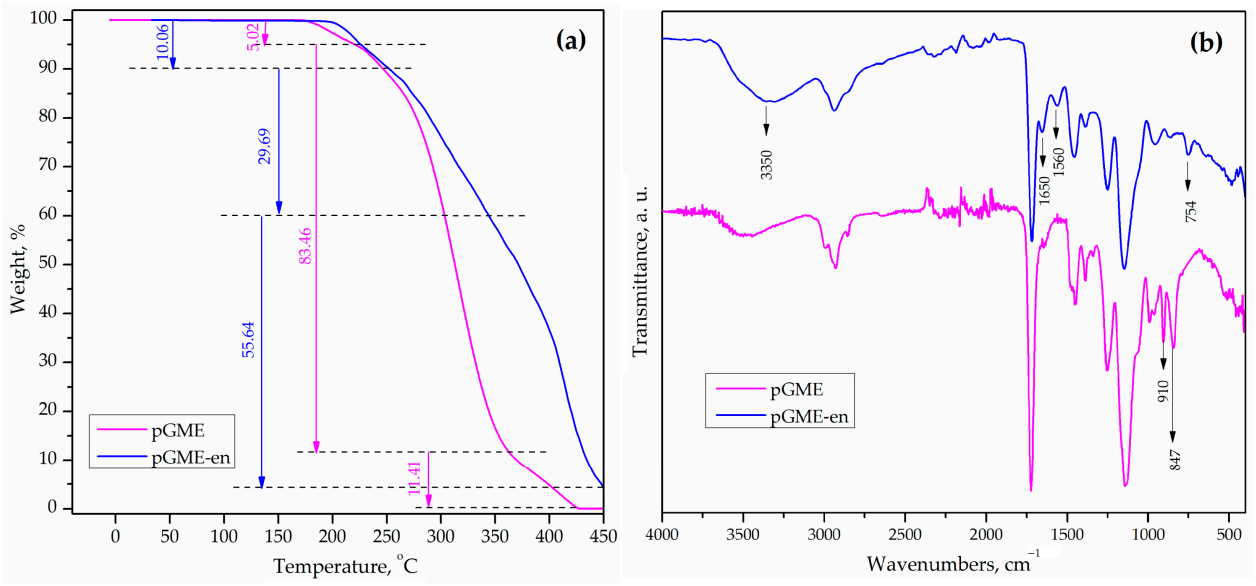

Figure 3. (**a**) TGA curves and (**b**) FTIR spectra of pGME and pGME-en.

The FTIR spectra of pGME and pGME-en are given in Figure 3b. The characteristic absorption bands at 2994, 2926, and 2852 cm^{-1}, assigned to $–CH_2$ and –CH– stretching vibrations as well as the bands of $–CH_2$ and –CH– bending vibrations at 1447 and 1386 cm^{-1}, were observed. In addition, epoxy ring vibrations at 1256, 910, and 847 cm^{-1}, such as stretching carbonyl vibrations at 1722 cm^{-1} peaks, were found [37,38]. Compared with the pGME spectrum, the appearance of new absorption bands was observed at 1656, 1561 (N–H bending vibrations), and 754 cm^{-1} (N–H wagging vibrations), as well as broad bands assigned to the –OH and to the N–H stretching vibrations, with a maximum at ~3400 cm^{-1} [37,39]. Also, a decreasing intensity of characteristic epoxy vibration peaks was observed. All these variations of absorption bands between the pGME and pGME-en confirm that the pGME had been successfully amino-functionalized with ethylene diamine.

The surface chemical composition of pGME-en was analyzed by XPS and the characteristic peaks for C 1s, O 1s, and N 1s were identified in the wide scan spectrum (Figure 4a). The presence of the N 1s peak at ~400 eV confirmed the amino-functionalization of pGME. For more detailed characterization, a high-resolution (HRES) spectrum of C 1s was employed.

Figure 4b shows the high-resolution C 1s spectra deconvoluted into three peaks. The low binding energy peak at 284.7 eV is attributed to carbon (C–C and C=C) and the other most intensive peak at 286.6 eV is assigned to bounded hydroxyl or amino groups [40]. The third peak at 288.7 eV is due to the presence of –COO [41]. The deconvolution of C 1s indicated that the amine group had been grafted onto the pGME-en surface, which was in agreement with the results obtained from FTIR analysis.

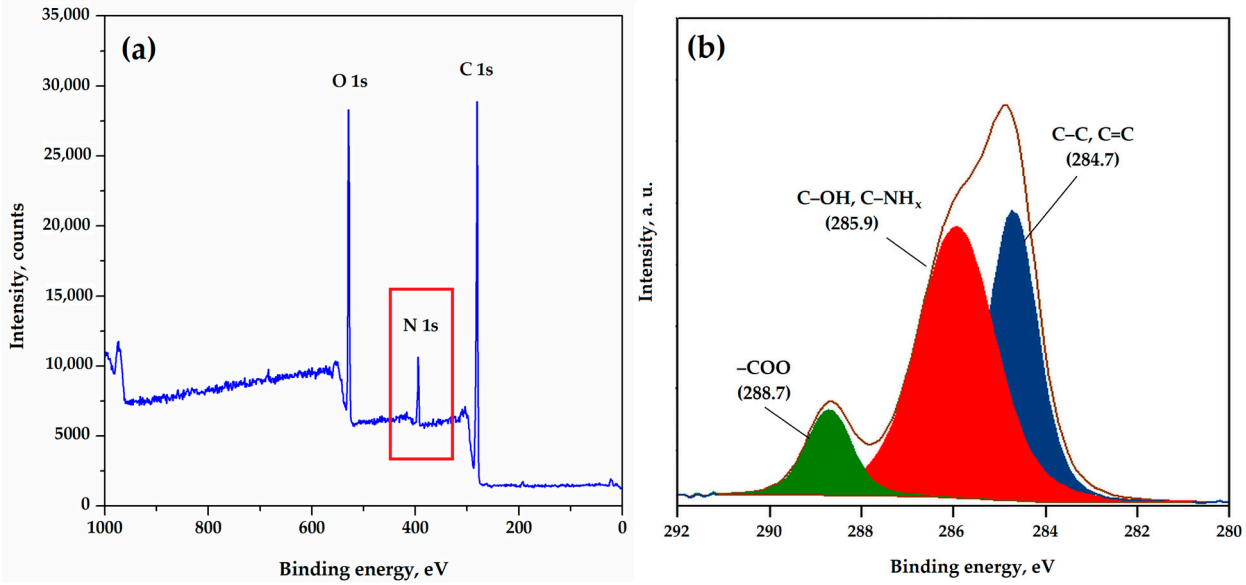

Figure 4. (**a**) XPS survey spectrum and (**b**) HRES C 1s spectrum of pGME-en.

3.2. Adsorption Kinetics

The results of the effect of contact time on Au adsorption onto pGME-en, in the contact time range of 1 to 180 min, are presented in Figure 5a. It can be seen that the adsorption of gold by pGME-en varies with time; it increases rapidly until approximately 20 min, then gradually attains equilibrium at 30 min, with a maximal capacity of 187.22 mg/g. The adsorption half time was 5 min, and after 30 min, only a negligible variation of adsorption capacity was noticed.

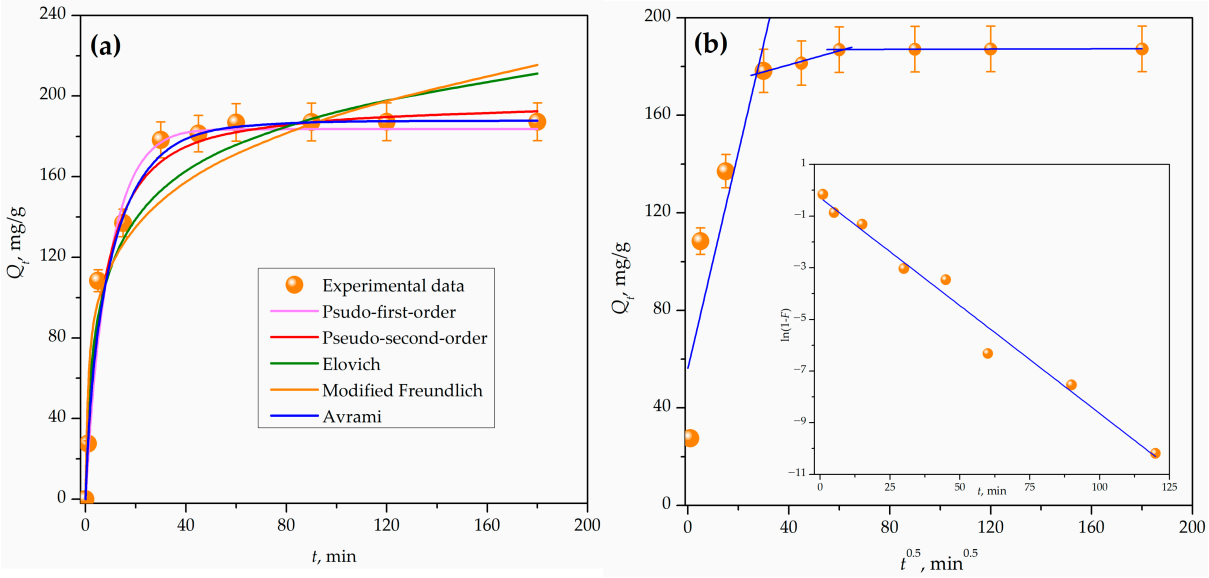

Figure 5. (**a**) Time-dependent adsorption plot with non-linear kinetic curves and (**b**) intra-particle diffusion plot for Au adsorption on pGME-en. Inset: The liquid film diffusion plot for Au adsorption.

In order to acquire information about the types of interactions between pGME-en and Au ions and elucidate the adsorption rate, the experimental data were evaluated using the following surface reaction-based kinetic models: pseudo-first-order (Equation (2)), pseudo-second-order (Equation (3)), Elovich (Equation (4)), modified Freundlich (Equation (5)), and Avrami kinetic models (Equation (6)) [42,43]. The kinetic parameters of the adsorption process were derived using non-linear regression fitting methods. The calculated kinetic

parameters and coefficients of determination (R^2) are listed in Table 2, while fitting curves are displayed in Figure 4a.

$$Q_t = Q_e\left(1 - e^{-k_1 t}\right) \tag{2}$$

$$Q_t = \frac{Q_e^2 k_2 t}{1 + Q_e k_2 t} \tag{3}$$

$$Q_t = \frac{1}{\beta}\ln(\alpha\beta t + 1) \tag{4}$$

$$Q_t = k_{MF} C_i t^{1/m} \tag{5}$$

$$Q_t = Q_e(1 - \exp[-k_{AV} t^n]) \tag{6}$$

where Q_t (mg/g) and Q_e (mg/g) are the adsorption capacity at time t and equilibrium, respectively, k_1 (1/min) is the adsorption-rate constant for the pseudo-first-order, k_2 (g/mg min) is the adsorption-rate constant for the pseudo-second-order, α (mg/g min) is the adsorption-rate constant related to chemisorption, β (g/mg) is the activation energy for chemisorption and is related to the extent of the surface, k_{MF} (L/g min) is the adsorption-rate constant for the modified Freundlich model, m is the Kuo–Lotse constant, k_{AV} (1/min) is the Avrami kinetic rate coefficient, and n is the Avrami model exponent of time, corresponding to the adsorption mechanism.

The highest value of the correlation coefficients (R^2) of the five surface models was 0.987 for the pseudo-second-order and Avrami models. The value of the calculated adsorption capacity for the Avrami kinetic model (187.80 mg/g) was found to be close to the experimentally obtained adsorption capacity (187.22 mg/g), indicating that the Avrami kinetic model better explained the adsorption of gold onto the pGME-en. The obtained results suggest that the adsorption process is complex and follows multiple kinetic orders that are changed during the contact of the gold with the active sites on pGME-en, depending on the affinity of the metal ions to the pGME-en. The adsorption of gold ions by the amino-functionalized copolymer may occur via electron sharing or ion exchange between active sites on the copolymer support and gold ions [44,45].

Since the experimental data fit very well to the Avrami model, the four diffusion-based kinetic models (liquid film diffusion (Equation (7)), intra-particle diffusion (Equation (8)), the Bangham model (Equation (9)), and the Boyd model (Equation (10))) were used to further understand the mechanism of Au adsorption onto pGME-en, as well as to determine the rate-controlling step of the processes [42]. The values of obtained diffusion-based kinetic parameters are represented in Table 2, while the results of the fitting results are shown in Figure 5b.

$$\ln(1 - F) = -k_{LFD} t + C_{LFD} \tag{7}$$

$$Q_t = k_{id} t^{0.5} + C_{id} \tag{8}$$

$$\log\log\left(\frac{C_i}{C_i - Q_t m}\right) = \log\frac{k_B m}{2.303V} + \alpha\log t \tag{9}$$

$$Bt = \left(\sqrt{\pi} - \sqrt{1 - \frac{\pi F}{3}}\right)^2 \text{ for } F < 0.85 Bt = -0.4977 - \ln(1 - F) \text{ for } F > 0.85 \tag{10}$$

where k_{LFD} (1/min) is the liquid film diffusion rate constant, $F = Q_t/Q_e$ is the equilibrium fractional attainment, k_{id} (mg/g min$^{0.5}$) is the intra-particle diffusion rate constant, C_{id} is

proportional to the thickness of the boundary layer, m (g/L) is the dosage of adsorbent, k_B (1/g) is the rate constant of Bangham model, α is the constant corresponding to the adsorption intensity, and Bt is a mathematical function of F.

Table 2. Kinetic parameters for gold adsorption by pGME-en.

Model	Parameter	Value
Pseudo-first-order	$Q_e{}^{calc}$, mg/g	183.67
	k_1, 1/min	0.13
	R^2	0.963
Pseudo-second-order	$Q_e{}^{calc}$, mg/g	197.87
	$k_2 \cdot 10^3$, g/mg min	1.01
	R^2	0.987
Elovich	α, mg/g min	136.29
	$\beta \cdot 10^2$, g/mg	3.15
	R^2	0.915
Modified Freundlich	$k_{MF} \cdot 10^2$, L/g min	3.75
	m	4.85
	R^2	0.842
Avrami	k_{AV}, 1/min	0.12
	n	0.74
	$Q_e{}^{calc}$, mg/g	187.80
	R^2	0.987
Liquid film diffusion	$k_{LFD} \cdot 10^2$, 1/min	8.35
	C_{LFD}	0.29
	R^2	0.982
Intra-particle diffusion	k_{Id}, mg/g min$^{0.5}$	3.78
	C_{id}	157.12
	R^2	0.959
Bangham	$k_B \cdot 10^3$, 1/g	0.47
	α	0.46
	R^2	0.861
Boyd	R^2	0.974

As shown in Figure 5b (inset), the straight line of the liquid film diffusion plot did not pass through the origin, indicating the involvement of pore diffusion in the mechanism of metal ion adsorption [46]. Bearing in mind that the ion diameter for non-covalent interactions would be slightly less than 12 Å (1.2 nm), it is expected that the $[AuCl_4]^-$ ion can penetrate through micro-, meso-, and macropores and that its binding inside the polymer also has a significant contribution to the sorption of this ion, not only on the surface. Brief analyses of the structural parameters for the $[AuCl_4]^-$ ion with the structure of the $[AuCl_4]^-$ anion (Figure S1) are given in the Supplementary Materials. The intra-particle plots (Figure 5b) show three distinct stages: a liquid film diffusion stage, an intra-particle diffusion stage, and a final equilibrium stage [37]. According to the obtained results, the intra-particle plots were linear and deviated from the origin, suggesting that the adsorption of Au onto pGME-en was controlled by both liquid film and intra-particle diffusion. These results are corroborated by the Bangham (Figure S2a) and Boyd (Figure S2b) plots, suggesting that diffusion through pores is not the predominant mechanism, since their curves did not pass the coordinate onset.

Previous research on gold adsorption reports various adsorbents that can recover this precious metal, such as activated carbon, different types of biosorbents, and functionalized magnetic nanoparticles [47–49]. However, variations in the experimental conditions, and the different properties of adsorbents, like surface chemistry and functional groups, make direct comparisons of the reported data difficult to achieve. The experimental adsorption

capacity and equilibrium adsorption time of pGME-en for gold removal obtained in this study were compared with several adsorbents recently reported in the literature listed in Table 3. As can be seen, pGME-en has a fast adsorption, i.e., the equilibrium adsorption time obtained in this study was 0.5 h, while the majority of sorbents listed in Table 3 have an equilibrium time of over 3 h.

Table 3. Comparison of various adsorbents for gold removal.

Adsorbent *	pH	Q_e^{exp}, mg/g	t_{eq}, h	Ref.
Fe_3O_4@SiO_2-NH_2	2	14.10	-	[50]
Amberlite XAD 7-L-glutamic acid	<4	14.23	1	[51]
DACS-TA	<5.7	298.5	22	[52]
RFT-SA	3	386.5	18	[53]
CPEIR	2	943.5	12	[54]
PE-PGMA	3	99.08	0.2	[55]
A-PGMA	4	201.214	3	[56]
pGME-en	1.5	187.22	0.5	This study

* Fe_3O_4@SiO_2-NH_2—amino-functionalized magnetic nanoparticles; Amberlite XAD 7-L-glutamic acid—Amberlite XAD 7 functionalized with L-glutamic acid; DACS-TA—tannin acid-immobilized dialdehyde corn starch; RFT-SA—resorcinol–formaldehyde–thiourea in sodium alginate hydrogels; CPEIR—crosslinked polyethyleneimine resins; PE-PGMA—trimethyl phosphate modified poly(glycidyl methacrylate); A-PGME—2-aminothiazole-functionalized poly(glycidyl methacrylate) microspheres.

3.3. The Mechanism of Gold Adsorption onto pGME-en

FTIR and XPS analyses of pGME-en before and after the gold adsorption were performed, in order to understand the mechanism of the adsorption process. FTIR spectra before and after gold adsorption are given in Figure 6a. The N–H bending vibration at ~1650 cm^{-1} was shifted towards lower wavenumbers (1630 cm^{-1}), while the band at ~1560 cm^{-1} disappeared from the spectrum after adsorption, indicating the formation of a C–N–Me bond. A similar result was reported in the literature [57]. Also, the shift and intensity decrease in the N–H wagging vibration peak, from 754 cm^{-1} to 750, can be observed. The C–O stretching band at 956 cm^{-1}, for the amino-modified copolymer, was shifted to ~980 cm^{-1}. At the same time, the intensity of the peak at 1450 cm^{-1} decreased. According to the literature, this can suggest that O atoms in –OH groups might also be involved in the metal adsorption process [58].

The XPS wide scan spectra of pGME-en before and after the adsorption of Au ions are presented in Figure 6b. The characteristics peaks for C 1s, O 1s, and N 1s were identified for both samples. After the gold adsorption, a new peak of Au 4f at 83.5 eV was observed, indicating Au bonding with reactive sites onto pGME-en. For further analysis, high-resolution (HRES) spectra of Au 4f, C 1s, N 1s, and O 1s were employed.

The Au 4f core-level spectrum (Figure 7a) had two peaks, corresponding to Au $4f_{7/2}$ (84.5 eV) and Au $4f_{5/2}$ (88.2 eV), with a spin-orbit splitting of 3.7 eV. The Au $4f_{7/2}$ was fitted into three components located at 84.6, 85.6, and 87.0 eV, corresponding to Au(III), Au(I), and metallic Au, respectively. The Au $4f_{5/2}$ peak had three components at a binding energy of 88.2, 89.4, and 90.6 eV, which implied the existence of +3, +1, and Au zero valence states on the pGME-en surface [59]. The presence of Au in higher valence states is due to the oxidation of the outermost layer of the gold nanoparticles. Also, it should be emphasized that an upshift of the Au $4f_{7/2}$ and Au $4f_{5/2}$ binding energy positions, relative to the bulk standard values, was observed. The presence of the support material altered the Au 4f binding energy positions, which is an indication of the interaction of the Au NPs with the surrounding chemical environment. This analysis leads to the conclusion that Au was immobilized on the surface of the pGME-en beads, in the form of Au metal. According to the HRES C 1s (Figure 7b) of pGME-en after adsorption, a new peak at 288.0 eV for C=O appeared, indicating the redox reaction presence during the Au adsorption onto pGME-en [54].

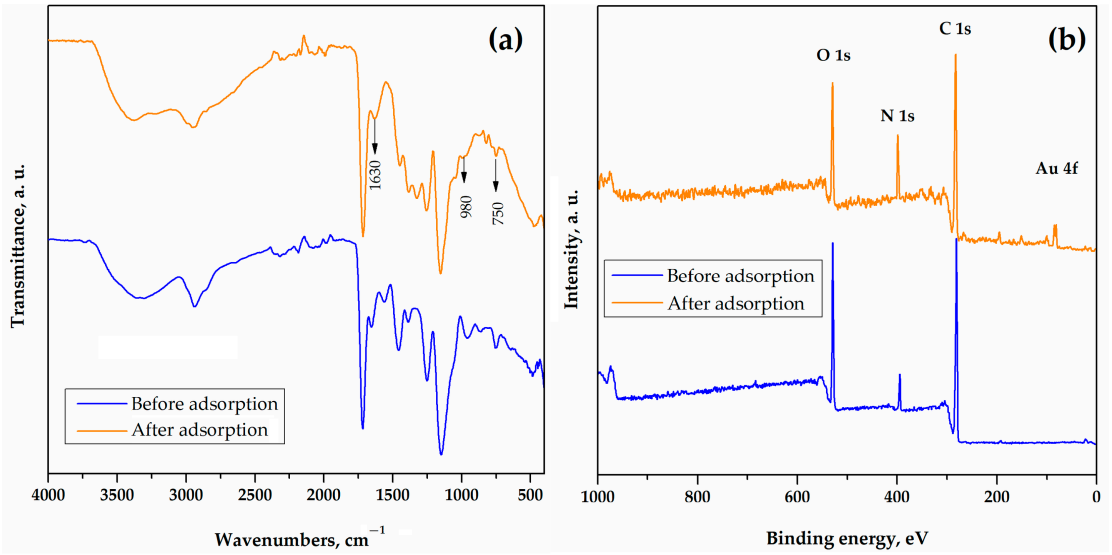

Figure 6. (**a**) FTIR spectra and (**b**) XPS survey spectra of pGME-en before and after gold adsorption.

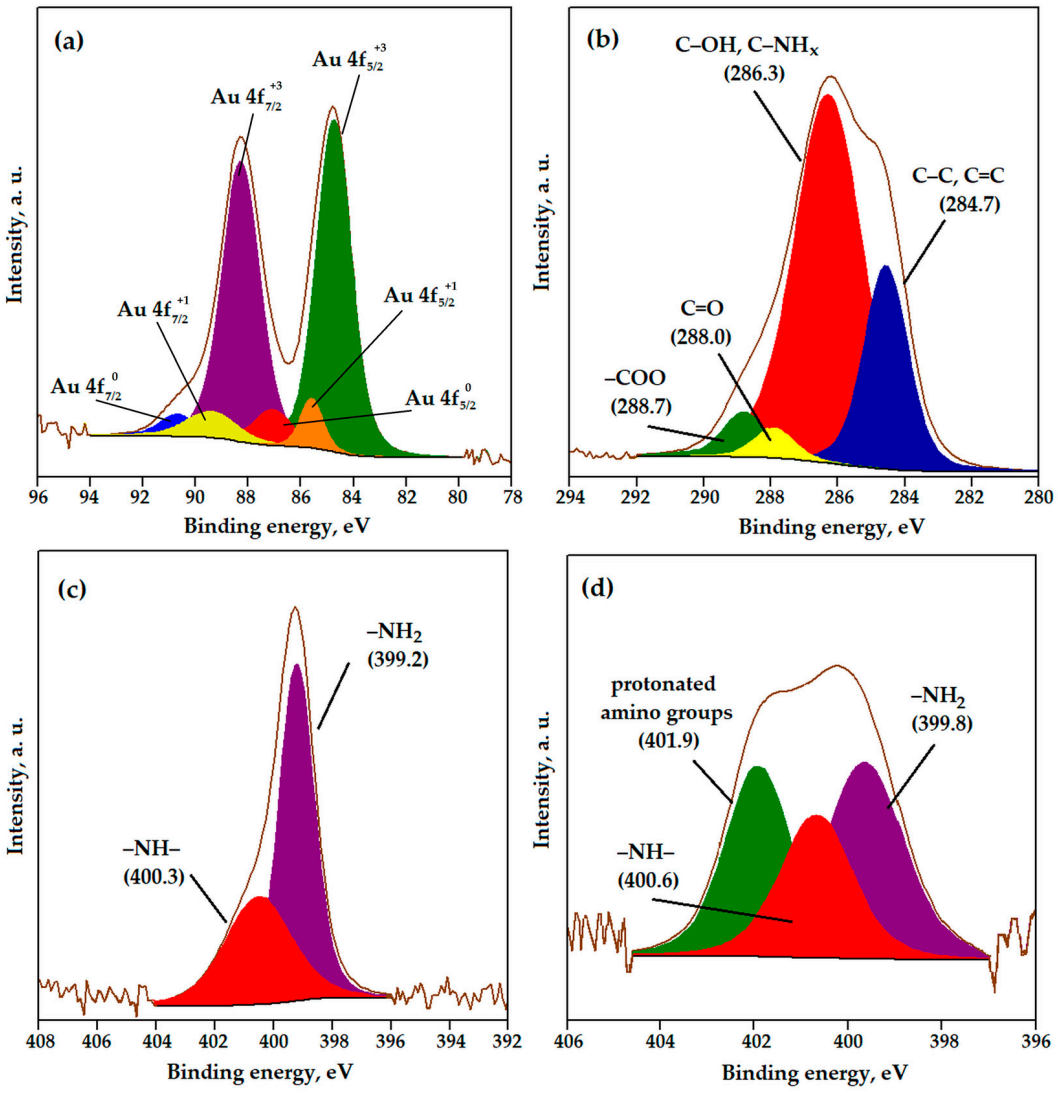

Figure 7. XPS spectra of pGME-en (**a**) HRES Au 4f, (**b**) HRES C 1s after, (**c**) HRES N 1s before, and (**d**) HRES N 1s after gold adsorption.

To investigate the involvement of amino and hydroxyl groups in adsorption, the N 1s and O 1s spectra were further analyzed. The N 1s core-level spectrum of the pGME-en copolymer (Figure 7c) was resolved into two nitrogen peaks, which corresponded to non-protonated $-NH_2$ (399.2 eV) and $-NH-$ (400.3 eV) [60]. After adsorption (Figure 7d), the spectra exhibited a new peak (401.9 eV) assigned to protonated amine groups, which indicated that amino groups are involved in the interaction with Au ions [61]. The O 1s core-level spectra of pGME-en before and after the adsorption of gold ions (Figure S3) were fitted with two peaks at ~531.6 and ~532.9 eV, corresponding to O=C and –OH, respectively [62]. After adsorption, the peak intensity assigned to hydroxyl groups increased, indicating that hydroxyl groups had interacted with the metal ions. The XPS data suggest that Au immobilization onto pGME-en proceeded via electrostatic interaction with protonated amine groups and/or through a complex formation mechanism with amino and hydroxyl groups (where nitrogen and/or oxygen act as the coordinating atoms). A possible mechanism of Au adsorption onto pGME-en is presented in Figure 8. A similar observation was made for Au adsorption by crosslinked polyethyleneimine resin [54].

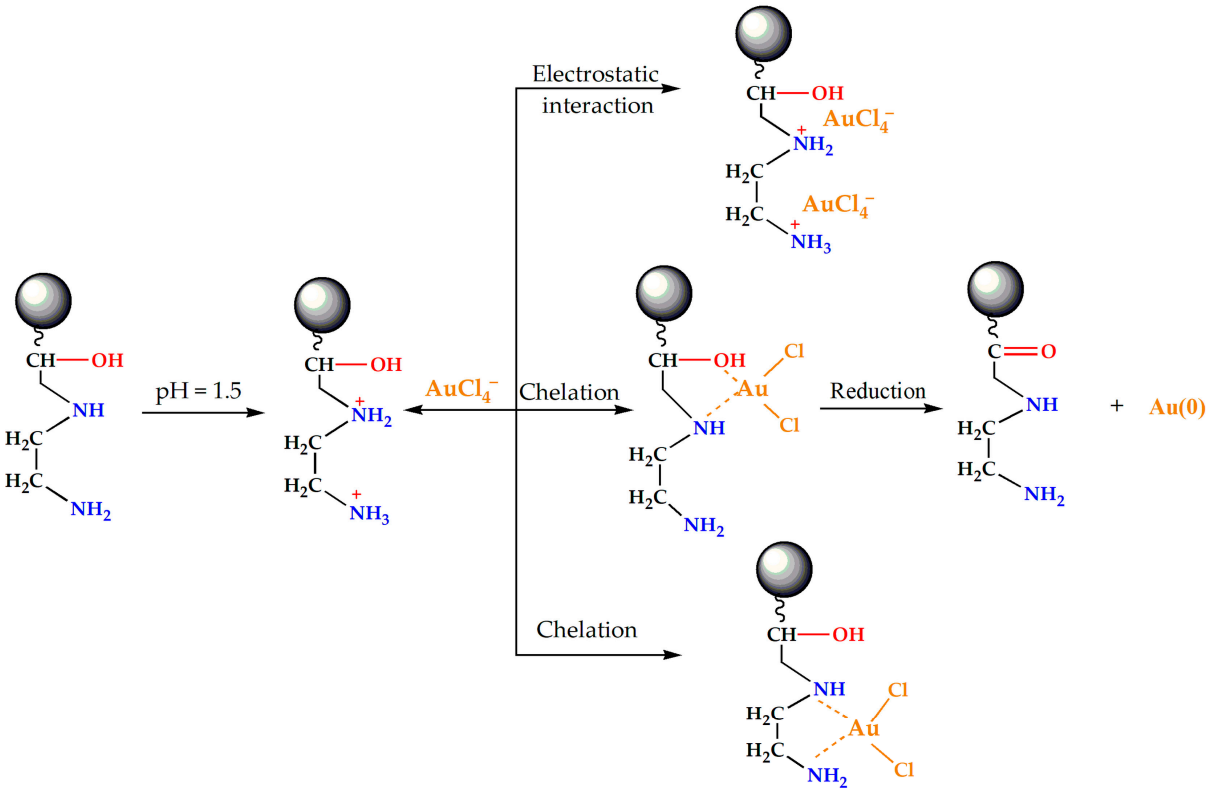

Figure 8. The possible Au adsorption mechanism onto pGME-en.

3.4. Characterization of Gold Polymer Composite

The use of pGME-en as an effective adsorbent for Au recovery from acid solutions gives the possibility for the preparation of functional gold polymer composite particles, via the reduction and deposition of Au(0) nanoparticles onto the pGME-en surface. Since gold nanoparticle-coated materials can be used in various applications, such as catalysis [16], antimicrobial nanocoatings [63], and water purification [64], a detailed characterization of obtained pGME-en/Au is needed.

The appearance of the particles and the surface morphology of the gold polymer composite was investigated by SEM and the obtained micrographs are depicted in Figure 9a,b. The SEM micrographs revealed the presence of grains of elemental gold, distributed on the surface of the pGME-en beads (bright aggregates). A strong peak (Figure 9c) was detected on the pGME-en/Au particle surface, with values of 0.52 *w*/*w*%.

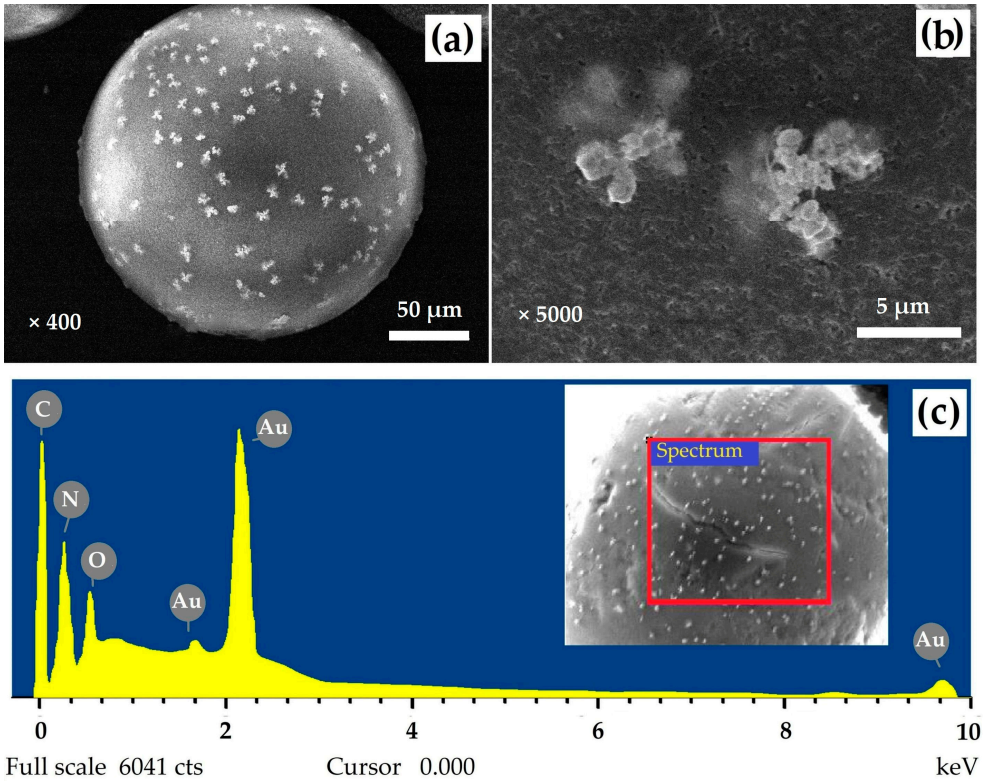

Figure 9. SEM micrographs of (**a**) particle beads (magnification × 400), and (**b**) surface (magnification × 5000). (**c**) EDS spectra of pGME-en/Au.

The porosity of PGME-en/Au was investigated by mercury porosimetry, and the results are presented in Figures S4 and 10a. The cumulative pore size distribution curve (Figure S4) did not have a plateau in the area of mesopores, which suggests the presence of mesopores and micropores in the pGME-en/Au sample. Also, a significant shift in the pore size distributions toward higher pore sizes for pGME-en/Au, in comparison to pGME-en, can be observed (Figure 10a), which decreased the value of the specific surface area. Namely, the pGME-en/Au had the value of a specific surface area of 42 m^2/g, while pGME-en had a twice as high $S_{s,Hg}$ value of 80 m^2/g.

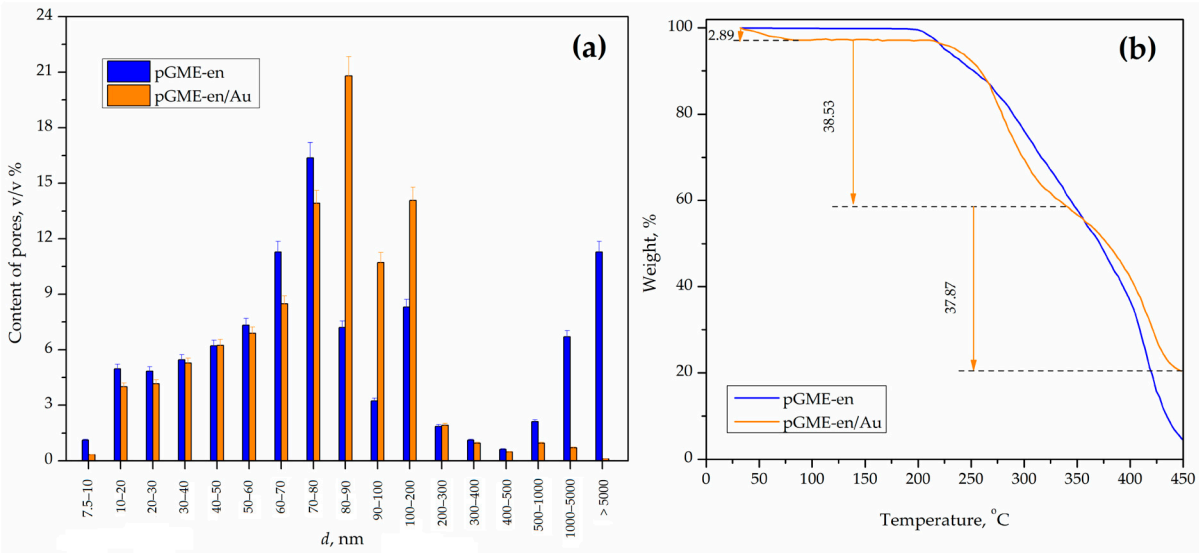

Figure 10. (**a**) The pore size distribution diagrams and (**b**) TGA curves of pGME-en and pGME-en/Au.

The thermal degradation of pGME-en/Au is presented in Figure 10b. It can be seen that pGME-en/Au exhibited a weight loss of about 5% below 100 °C, due to the loss of water physically adsorbed or occluded in the pores [65]. Then, the degradation of pGME-en/Au took place in two stages. The first stage, for a copolymer with immobilized Au, took place between 210 °C and 340 °C and the second one was in the range between 340 and 450 °C. The main degradation mechanism of pGME-en/Au was depolymerization into oligomers and monomers, initiated by the cleavage of weak linkages, ester decomposition and the elimination of the amine groups that simultaneously occur [27,36]. Also, the T_i value of PGME-en/Au was approximately 20 °C higher than the T_i value of pGME-en, suggesting a slight increase in thermal stability.

The release study was undertaken through static experiments in a physiological solution over 24 h, to detect and measure the amounts of Au that can be released from the gold polymer composite and diffused into surrounding medium, in order to simulate the material performances under real conditions. The results are shown in Figure 11. As can be seen, pGME-en/Au released almost the same amount of Au ions (1.75 mg/g) after 1 h and 3 h, with a maximum concentration of released ions of 2.2 mg/g after 24 h.

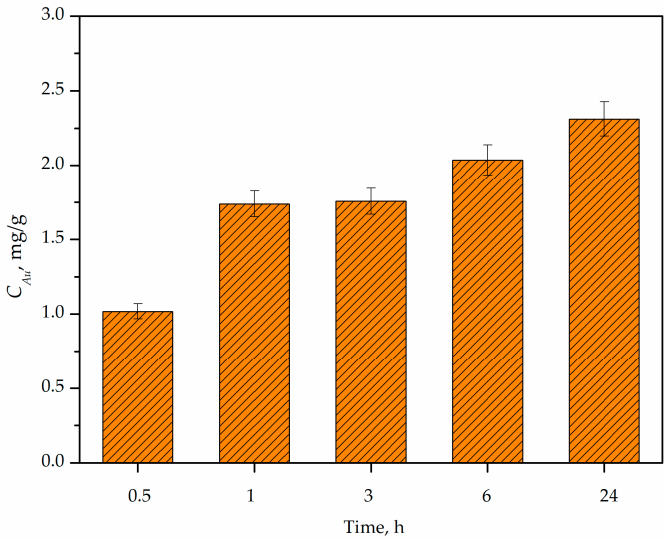

Figure 11. Release of Au ions from gold polymer composite into physiological saline solution.

3.5. Antimicrobial Evaluation of Gold Polymer Composite

In this study, the selected Gram-positive and Gram-negative bacteria and yeast were used to investigate the antimicrobial activity of the gold polymer composite. The ability of the pGME-en/Au to inhibit the growth of the tested microorganisms is presented in Table 4 and Figure 12.

Table 4. Antimicrobial effects of gold polymer composite against selected bacteria and fungi (inhibition zone around wells containing 10 mg of materials suspension).

Test Organism	Inhibition Zone (ϕ mm)
Staphylococcus aureus ATCC [a] 25923	7.5
Listeria monocytogenes NCTC [b] 11994	9.0
Escherichia coli NCTC 2001	-
Candida albicans ATCC 10231	8.0

[a] ATCC—American Type Culture Collection. [b] NCTC—National Collection of Type Cultures.

Figure 12. Zone of inhibition of gold-based composite against *C. albicans*.

As seen, the investigated material showed antimicrobial properties against two Gram-positive bacterial strains and *C. albicans*, while any noticeable antibacterial activity against *E. coli* was not detected. The largest inhibition zone was registered against *L. monocytogenes* (9 mm). The different activity of pGME-en/Au toward *E. coli* and *S. aureus* can be explained by the differences in their cell walls. Namely, *E. coli*, as a Gram-negative bacteria, has an additional membrane with a bilayer phospholipid structure, protecting the cell from penetration of biocides into the cytoplasm; *S. aureus*, as a Gram-positive bacteria, is more affected by composite, since it has a loosely packed polyglycane outer layer, which facilitates the deep penetration of biocide inside the cell and an interaction with the cytoplasmic membrane [31,66].

Different doses of composite (20, 10, and 5 mg) were used to assess the dose dependence of the antimicrobial activity against *C. albicans*. From Figure 12, it can be seen that the inhibition zone increased with an increasing dose of pGME-en/Au. Preliminary results indicated that the water-insoluble gold polymer composite, with a tunable particle size and surface chemistry, can be considered as a potential antibacterial material and may be able to be used to inhibit bacterial growth in various industrial and biomedical applications, such as water purification, wound dressings, bacterial responsive coatings, etc. [64,67]. Further investigations will focus on improving the antimicrobial efficiency, to design recyclable and reusable materials with long-lasting responses.

4. Conclusions

The primary objective of this study was to develop a technique that would allow for the recovery of gold and the subsequent use of this versatile sorbent as an antimicrobial agent. A novel porous pGME-en was tested as a potential adsorbent for gold from aqueous solutions in a simple adsorption procedure. The main pGME-en performance is fast gold adsorption, with an adsorption half-time of 5 min and a maximal adsorption capacity of about 187 mg/g, achieving an equilibrium time of 30 min. The best fit of Au adsorption kinetics was obtained with the pseudo-second-order and Avrami kinetic models (R^2 = 0.987), suggesting that the overall Au adsorption process is complex and follows multiple kinetic orders, that are changed during the contact of the gold with the active sites on pGME-en. The two diffusion steps, i.e., liquid film and intra-particle diffusion, controlled the Au adsorption onto pGME-en.

The gold polymer composite exhibits an altered porous structure and an increased initial degradation temperature. The main degradation mechanism of the composite is depolymerization to oligomers and monomers, initiated by the scission of weak linkages and ester decomposition. The XPS and FTIR analysis suggest Au complexation through the formation of Me–O and Me–N bonds with the -OH, -NH and -NH_2 groups as the possible

mechanism of Au immobilization on pGME-en. Also, XPS spectra of the pGME-en after adsorption pointed to the presence of a metallic form of zero valent Au and Au(III), indicating that Au(III) adsorption was followed by a partial reduction to Au(0) on the pGME-en surface. Preliminary antimicrobial tests suggest that the gold polymer composite has promising inhibitory activity and may be a potent antibacterial and antifungal candidate.

Supplementary Materials: The following supporting information can be downloaded at: https://www.mdpi.com/article/10.3390/met13111864/s1, Figure S1: the structure of the $[AuCl_4]^-$ anion, with measured Au-Cl bond lengths; Figure S2: (a) Bangham and (b) Boyd plots for Au adsorption on pGME-en; Figure S3: HRES O 1s spectra of pGME-en (a) before and (b) after gold adsorption; Figure S4: cumulative pore size distribution curve for pGME-en/Au. References [68,69] are cited in the supplementary materials.

Author Contributions: Conceptualization, A.N.; methodology, A.N. and A.O.; carrying out measurements, Z.V., P.S. and D.M.; investigation, T.T.; data curation, B.M.; writing—original draft preparation, A.N.; writing—review and editing, B.M., P.S., D.M. and T.T.; visualization, B.M.; supervision, A.O.; funding acquisition, A.N. All authors have read and agreed to the published version of the manuscript.

Funding: This work was financially supported by the Ministry of Science, Technological Development and Innovation of the Republic of Serbia (contracts: 451-03-47/2023-01/200026, 451-03-47/2023-01/200135, and 451-03-47/2023-01/200017) and the European Regional Development Fund—Operational Programme Science and Education for Smart Growth (BG05M2OP001-1.001-0008).

Data Availability Statement: The data presented in this study are available on request from the corresponding author.

Acknowledgments: The authors want to express their sincere thanks to Sandra Bulatović (University of Belgrade, Institute of Chemistry, Technology and Metallurgy) and Jasmina Nikodinović-Runić (University of Belgrade, Institute of Molecular Genetics and Genetic Engineering) for their insightful help in discussions of antimicrobial test results. Also, the authors want to express their special thanks to Goran Janjić (University of Belgrade, Institute of Chemistry, Technology and Metallurgy) for their help calculating structural parameters for the $[AuCl_4]^-$ ion.

Conflicts of Interest: The authors declare that they have no known competing financial interests or personal relationships that could have appeared to influence the work reported in this paper.

References

1. Syed, S. Recovery of Gold from Secondary Sources—A Review. *Hydrometallurgy* **2012**, *115–116*, 30–51.
2. Yuan, W.; Chen, X.; Xu, Y.; Yan, C.; Liu, Y.; Lian, W.; Zhou, Y.; Li, Z. Preparation and Recyclable Catalysis Performance of Functional Macroporous polyHIPE Immobilized with Gold Nanoparticles on Its Surface. *RSC Adv.* **2018**, *8*, 5912–5919. [PubMed]
3. Gökelma, M.; Birich, A.; Stopic, S.; Friedrich, B. A Review on Alternative Gold Recovery Re-Agents to Cyanide. *J. Mater. Sci. Chem. Eng.* **2016**, *04*, 8–17.
4. Wang, C.; Lin, G.; Zhao, J.; Wang, S.; Zhang, L.; Xi, Y.; Li, X.; Ying, Y. Highly Selective Recovery of Au(III) from Wastewater by Thioctic Acid Modified Zr-MOF: Experiment and DFT Calculation. *Chem. Eng. J.* **2020**, *380*, 122511.
5. Guo, J.; Luo, X.; Tan, S.; Ogunseitan, O.A.; Xu, Z. Thermal Degradation and Pollutant Emission from Waste Printed Circuit Boards Mounted with Electronic Components. *J. Hazard. Mater.* **2020**, *382*, 121038.
6. Forti, V.; Baldé, C.P.; Kuehr, R.; Bel, G. *The Global E-Waste Monitor 2020: Quantities, Flows and the Circular Economy Potential*; United Nations University/United Nations Institute for Training and Research: Bonn, Germany; International Telecommunication Union: Geneva, Switzerland; International Solid Waste Association: Rotterdam, The Netherlands, 2020.
7. Zhao, W.; Yang, B.; Yi, Y.; Feng, Q.; Liu, D. Synergistic Activation of Smithsonite with Copper-Ammonium Species for Enhancing Surface Reactivity and Xanthate Adsorption. *Int. J. Min. Sci. Technol.* **2023**, *33*, 519–527. [CrossRef]
8. Shen, Z.; Wen, S.; Wang, H.; Miao, Y.; Wang, X.; Meng, S.; Feng, Q. Effect of Dissolved Components of Malachite and Calcite on Surface Properties and Flotation Behavior. *Int. J. Miner. Metall. Mater.* **2023**, *30*, 1297–1309.
9. Dangi, Y.R.; Bediako, J.K.; Lin, X.; Choi, J.-W.; Lim, C.-R.; Song, M.-H.; Han, M.; Yun, Y.-S. Polyethyleneimine Impregnated Alginate Capsule as a High Capacity Sorbent for the Recovery of Monovalent and Trivalent Gold. *Sci. Rep.* **2021**, *11*, 17836.
10. Dzhardimalieva, G.I.; Uflyand, I.E. Synthetic Methodologies for Chelating Polymer Ligands: Recent Advances and Future Development. *ChemistrySelect* **2018**, *3*, 13234–13270.
11. Huang, P.; Zhang, Y.; Wang, B.; Zhu, X.; He, Y.; Song, P.; Wang, Z.; Wang, R. Synthesis of Acryloyl Copolymer Core–Shell Microspheres with Antibacterial Activity and Surface Cationic Effects. *J. Mater. Sci.* **2023**, *58*, 7718–7730.

12. Liu, J.; Wang, N.; Liu, J.; Li, M.; Xu, Y.; Wang, C.; Wang, Y.; Zheng, H.; Ma, L. The Immobilization of Pd(II) on Porous Organic Polymers for Semihydrogenation of Terminal Alkynes. *ACS Appl. Mater. Interfaces* **2020**, *12*, 51428–51436. [CrossRef] [PubMed]
13. Marković, B.M.; Vuković, Z.M.; Spasojević, V.V.; Kusigerski, V.B.; Pavlović, V.B.; Onjia, A.E.; Nastasović, A.B. Selective Magnetic GMA Based Potential Sorbents for Molybdenum and Rhenium Sorption. *J. Alloys Compd.* **2017**, *705*, 38–50.
14. Mehdinia, A.; Salamat, M.; Jabbari, A. Preparation of a Magnetic Polystyrene Nanocomposite for Dispersive Solid-Phase Extraction of Copper Ions in Environmental Samples. *Sci. Rep.* **2020**, *10*, 3279. [CrossRef]
15. Poupart, R.; Grande, D.; Carbonnier, B.; Le Droumaguet, B. Porous Polymers and Metallic Nanoparticles: A Hybrid Wedding as a Robust Method toward Efficient Supported Catalytic Systems. *Prog. Polym. Sci.* **2019**, *96*, 21–42. [CrossRef]
16. Pourjavadi, A.; Kohestanian, M.; Keshavarzi, N. Immobilization of Au Nanoparticles on Poly(Glycidyl Methacrylate)-functionalized Magnetic Nanoparticles for Enhanced Catalytic Application in the Reduction of Nitroarenes and Suzuki Reaction. *Appl. Organomet. Chem.* **2020**, *34*, e5828. [CrossRef]
17. Trofin, M.; Racovita, S.; Vasiliu, S.; Bargan, A.; Bucatariu, F.; Vasiliu, A.; Mihai, M. Synthesis of Crosslinked Microparticles Based on Glycidyl Methacrylate and *N*-Vinylimidazole. *Macromol. Chem. Phys.* **2023**, 2300253. [CrossRef]
18. Suručić, L.T.; Nastasović, A.B.; Onjia, A.E.; Janjić, G.V.; Rakić, A.A. Design of Amino-Functionalized Chelated Macroporous Copolymer [Poly(GMA-EDGMA)] for the Sorption of Cu (II) Ions. *J. Serb. Chem. Soc.* **2019**, *84*, 1391–1404. [CrossRef]
19. Vasiliu, S.; Lungan, M.; Racovita, S.; Popa, M. Porous Microparticles Based on Methacrylic Copolymers and Gellan as Drug Delivery Systems. *Polym. Int.* **2020**, *69*, 1066–1080. [CrossRef]
20. Melo, C.; Silva, L.; Costa, L.; Marques, M. Synergistic Effect of Adsorption and Enzymatic Conversion in the Bisphenol-A Removal by Laccase Immobilized on Poly(Glycidyl Methacrylate-Co-Ethyleneglycol Dimethacrylate). *J. Braz. Chem. Soc.* **2017**, *28*, 2192–2201. [CrossRef]
21. Zhang, J.; Man, H.; Han, X.; Wang, Z.; Jiang, Y. Facile Preparation of Magnetic P(MMA-Co-GMA)@Fe_3O_4@PMAA Microspheres Using Porous Microsphere as Templates for Removal of Methylene Blue. *Colloid Polym. Sci.* **2023**, *301*, 933–947. [CrossRef]
22. Xie, W.; Xiong, Y.; Wang, H. Fe_3O_4-Poly(AGE-DVB-GMA) Composites Immobilized with Guanidine as a Magnetically Recyclable Catalyst for Enhanced Biodiesel Production. *Renew. Energy* **2021**, *174*, 758–768. [CrossRef]
23. Jovanović, S.M.; Nastasović, A.; Jovanović, N.N.; Jeremić, K. Targeted Porous Structure of Macroporous Copolymers Based on Glycidyl Methacrylate. *MSF* **1996**, *214*, 155–162.
24. Ekmeščić, B.M.; Maksin, D.D.; Marković, J.P.; Vuković, Z.M.; Hercigonja, R.V.; Nastasović, A.B.; Onjia, A.E. Recovery of Molybdenum Oxyanions Using Macroporous Copolymer Grafted with Diethylenetriamine. *Arab. J. Chem.* **2019**, *12*, 3628–3638. [CrossRef]
25. Jovanović, S.; Nastasović, A. Macroporous Glycidyl Methacrylate Copolymers, Synthesis, Characterization and Application. In *Polymeric Materials*; Nastasović, A., Ed.; Transworld Research Network: Kerala, India, 2009; pp. 1–27.
26. Marković, B.M.; Maksin, D.D.; Mojović, Z.D.; Vuković, Z.M.; Nastasović, A.B.; Jovanović, D.M. Electrochemical Behavior of Palladium Modified Amino-Functionalized Macroporous Copolymer. *J. Electroanal. Chem.* **2017**, *786*, 94–101. [CrossRef]
27. Marković, B.M.; Stefanović, I.S.; Nastasović, A.B.; Sandić, Z.P.; Suručić, L.T.; Dapčević, A.; Džunuzović, J.V.; Jagličić, Z.; Vuković, Z.M.; Pavlović, V.B.; et al. Novel Magnetic Polymer/Bentonite Composite: Characterization and Application for Re(VII) and W(VI) Adsorption. *Sci. Sinter.* **2021**, *53*, 419–428. [CrossRef]
28. Nastasović, A.; Jovanović, S.; Jakovljević, D.; Stanković, S.; Onjia, A. Noble Metal Binding on Macroporous Poly(GMA-Co-EGDMA) Modified with Ethylenediamine. *J. Serb. Chem. Soc.* **2004**, *69*, 455–460. [CrossRef]
29. Suručić, L.; Tadić, T.; Janjić, G.; Marković, B.; Nastasović, A.; Onjia, A. Recovery of Vanadium (V) Oxyanions by a Magnetic Macroporous Copolymer Nanocomposite Sorbent. *Metals* **2021**, *11*, 1777. [CrossRef]
30. Ebraheem, K.A.K.; Mubarak, M.S.; Yassien, Z.J.; Khalili, F. Chelation Properties of Poly(8–Hydroxyquinoline 5,7–Diylmethylene) Crosslinked with Bisphenol–A Toward Lanthanum(III), Cerium(III), Neodimium(III), Samarium(III), and Gadolinium(III) Ions. *Sep. Sci. Technol.* **2000**, *35*, 2115–2125. [CrossRef]
31. Palza, H. Antimicrobial Polymers with Metal Nanoparticles. *Int. J. Mol. Sci.* **2015**, *16*, 2099–2116. [CrossRef]
32. Erol, İ.; Özer, M. Copolymers of a Novel Amphiphilic Methacrylate Monomer Based on the Hydroxyl Group: Copolymerization Kinetics, Thermal Properties, Biological Activity, and Swelling Behavior. *J. Polym. Res.* **2021**, *28*, 372. [CrossRef]
33. Hanaa, D.; Youssef, A.; El-Metwally, E.; Abdelaal, M. Preparation and Characterization of Novel Poly(MMA-Co-GMA)/Ag Nanocomposites for Biomedical Applications. *Egypt. J. Chem.* **2019**, *62*, 2245–2252. [CrossRef]
34. Vukoje, I.D.; Džunuzović, E.S.; Vodnik, V.V.; Dimitrijević, S.; Ahrenkiel, S.P.; Nedeljković, J.M. Synthesis, Characterization, and Antimicrobial Activity of Poly(GMA-Co-EGDMA) Polymer Decorated with Silver Nanoparticles. *J. Mater. Sci.* **2014**, *49*, 6838–6844. [CrossRef]
35. Malović, L.; Nastasović, A.; Sandić, Z.; Marković, J.; Đorđević, D.; Vuković, Z. Surface Modification of Macroporous Glycidyl Methacrylate Based Copolymers for Selective Sorption of Heavy Metals. *J. Mater. Sci.* **2007**, *42*, 3326–3337. [CrossRef]
36. Marković, B.; Spasojević, V.; Dapčević, A.; Vuković, Z.; Pavlović, V.; Randjelović, D.; Nastasović, A. Characterization of Glycidyl Methacrylate Based Magnetic Nanocomposites. *Hem. Ind.* **2019**, *73*, 25–35. [CrossRef]
37. Suručić, L.; Janjić, G.; Marković, B.; Tadić, T.; Vuković, Z.; Nastasović, A.; Onjia, A. Speciation of Hexavalent Chromium in Aqueous Solutions Using a Magnetic Silica-Coated Amino-Modified Glycidyl Methacrylate Polymer Nanocomposite. *Materials* **2023**, *16*, 2233. [CrossRef]

38. Mujbil, H.H.; Al Jebur, L.A.; Yousif, E.; Kadhom, M.; Mohammed, A.; Ahmed, D.S.; Ali, M.; Hashim, H. Utilization of Metal Oxides Nanoparticles in Modulating Polyvinyl Chloride Films to Resist Ultraviolet Light. *Metals* **2022**, *12*, 1413. [CrossRef]
39. Martins, T.R.; Costa, P.S.; Bertuol, D.A.; Aguiar, M.L.; Tanabe, E.H. Development of Recycled Expanded Polystyrene Nanofibers Modified by Chitosan for the Removal of Lead(II) from Water. *Metals* **2022**, *12*, 1334. [CrossRef]
40. Qin, M.; Zong, S.; Zhang, P.; Li, J. Sustainable Route for Synthesis of Nitrogen-Doped Carbon Dots with High Efficiency for Iron(III) and Copper(II) Ions Detection. *J. Mater. Sci.* **2023**, *58*, 7559–7570. [CrossRef]
41. Rezaei, A.; Hadian-Dehkordi, L.; Samadian, H.; Jaymand, M.; Targhan, H.; Ramazani, A.; Adibi, H.; Deng, X.; Zheng, L.; Zheng, H. Pseudohomogeneous Metallic Catalyst Based on Tungstate-Decorated Amphiphilic Carbon Quantum Dots for Selective Oxidative Scission of Alkenes to Aldehyde. *Sci. Rep.* **2021**, *11*, 4411. [CrossRef]
42. Nastasović, A.; Marković, B.; Suručić, L.; Onjia, A. Methacrylate-Based Polymeric Sorbents for Recovery of Metals from Aqueous Solutions. *Metals* **2022**, *12*, 814. [CrossRef]
43. Fouad, M. Validation of Adsorption-Desorption Kinetic Models for Fipronil and Thiamethoxam Agrichemicals on Three Soils in Egypt. *Egypt. J. Chem.* **2022**, *66*, 219–222. [CrossRef]
44. Cheng, Y.; Chen, R.; Wang, P.; Wang, Q.; Wan, S.; Huang, S.; Su, R.; Song, Y.; Yang, X.; Fu, X. Synthesis of a Novel Biochar-Supported Polycarboxylic Acid-Functionalized Nanoiron Oxide-Encapsulated Composite for Wastewater Treatment: Removal of Cd(II), EDTA and Cd-EDTA. *J. Mater. Sci.* **2021**, *56*, 18031–18049. [CrossRef]
45. Zubieta, C.E.; Messina, P.V.; Luengo, C.; Dennehy, M.; Pieroni, O.; Schulz, P.C. Reactive Dyes Remotion by Porous TiO_2-Chitosan Materials. *J. Hazard. Mater.* **2008**, *152*, 765–777. [CrossRef] [PubMed]
46. Lin, X.; Wang, L.; Jiang, S.; Cui, L.; Wu, G. Iron-Doped Chitosan Microsphere for As(III) Adsorption in Aqueous Solution: Kinetic, Isotherm and Thermodynamic Studies. *Korean J. Chem. Eng.* **2019**, *36*, 1102–1114. [CrossRef]
47. Aghaei, E.; Alorro, R.; Encila, A.; Yoo, K. Magnetic Adsorbents for the Recovery of Precious Metals from Leach Solutions and Wastewater. *Metals* **2017**, *7*, 529. [CrossRef]
48. Seyedhakimi, A.; Bastami, S.A.; Ghassa, S.; Razavi, H.; Chehreh Chelgani, S. Exploring Relationships between Various Activations of Granular Activated Carbon on Silver and Gold Adsorption: A Kinetic and Equilibrium Study. *Sep. Sci. Technol.* **2019**, *54*, 1710–1721. [CrossRef]
49. Pan, H.-W.; Iizuka, A.; Shibata, E. Gold Recovery from Dilute Aqueous Solution by a Biosorbent Derived from Woody Biomass. *Chem. Eng. Commun.* **2021**, *208*, 1711–1724. [CrossRef]
50. Geng, Y.; Li, J.; Lu, W.; Wang, N.; Xiang, Z.; Yang, Y. Au(III), Pd(II) and Pt(IV) Adsorption on Amino-Functionalized Magnetic Sorbents: Behaviors and Cycling Separation Routines. *Chem. Eng. J.* **2020**, *381*, 122627. [CrossRef]
51. Mihăilescu, M.; Negrea, A.; Ciopec, M.; Davidescu, C.M.; Negrea, P.; Duţeanu, N.; Rusu, G. Gold (III) Adsorption from Dilute Waste Solutions onto Amberlite XAD7 Resin Modified with L-Glutamic Acid. *Sci. Rep.* **2019**, *9*, 8757. [CrossRef]
52. Liu, F.; Peng, G.; Li, T.; Yu, G.; Deng, S. Au(III) Adsorption and Reduction to Gold Particles on Cost-Effective Tannin Acid Immobilized Dialdehyde Corn Starch. *Chem. Eng. J.* **2019**, *370*, 228–236. [CrossRef]
53. Xiang, Y.; Liu, Y.; Li, M.; Bai, W.; Liu, G.; Xu, L. The Recovery of Au(III) by Hydrogel-like Beads. *Hydrometallurgy* **2023**, *215*, 105964. [CrossRef]
54. Liu, F.; Zhou, L.; Wang, W.; Yu, G.; Deng, S. Adsorptive Recovery of Au(III) from Aqueous Solution Using Crosslinked Polyethyleneimine Resins. *Chemosphere* **2020**, *241*, 125122. [CrossRef] [PubMed]
55. Xiong, C.; Wang, S.; Zhang, L. Selective Recovery Mechanism of Au(III) from an Aqueous Solution by Trimethyl Phosphate Modified Poly(Glycidyl Methacrylate). *J. Taiwan Inst. Chem. Eng.* **2019**, *95*, 55–64. [CrossRef]
56. Xiong, C.; Wang, S.; Zhang, L.; Li, Y.; Zhou, Y.; Peng, J. Preparation of 2-Aminothiazole-Functionalized Poly(Glycidyl Methacrylate) Microspheres and Their Excellent Gold Ion Adsorption Properties. *Polymers* **2018**, *10*, 159. [CrossRef] [PubMed]
57. Mohabey, H. IR Spectra, Magnetic and Thermal Studies of Copper (II) Complex of N-Hydroxy-N-(4-Chloro) Phenyl N'(4-Fluoro) Phenyl Benzamidine Hydrochloride. *Mat. Sci. Res. India* **2014**, *11*, 63–65. [CrossRef]
58. Xu, L.; Liu, Y.; Wang, J.; Tang, Y.; Zhang, Z. Selective Adsorption of Pb^{2+} and Cu^{2+} on Amino-Modified Attapulgite: Kinetic, Thermal Dynamic and DFT Studies. *J. Hazard. Mater.* **2021**, *404*, 124140. [CrossRef]
59. Xu, H.; Zhou, K.; Si, J.; Li, C.; Luo, G. A Ligand Coordination Approach for High Reaction Stability of an Au–Cu Bimetallic Carbon-Based Catalyst in the Acetylene Hydrochlorination Process. *Catal. Sci. Technol.* **2016**, *6*, 1357–1366. [CrossRef]
60. Ravi, S.; Zhang, S.; Lee, Y.-R.; Kang, K.-K.; Kim, J.-M.; Ahn, J.-W.; Ahn, W.-S. EDTA-Functionalized KCC-1 and KIT-6 Mesoporous Silicas for Nd^{3+} Ion Recovery from Aqueous Solutions. *J. Ind. Eng. Chem.* **2018**, *67*, 210–218. [CrossRef]
61. Prabhakar, M.N.; Raghavendra, G.M.; Vijaykumar, B.V.D.; Patil, K.; Seo, J.; Jung-il, S. Synthesis of a Novel Compound Based on Chitosan and Ammonium Polyphosphate for Flame Retardancy Applications. *Cellulose* **2019**, *26*, 8801–8812. [CrossRef]
62. Zhao, J.; Liu, X.; Ren, X.; Du, B.; Kuang, X.; Tian, D.; Wei, Q.; Wu, D. Chromium Doping: A New Approach to Regulate Electronic Structure of Cobalt Carbonate Hydroxide for Oxygen Evolution Improvement. *J. Colloid Interface Sci.* **2022**, *609*, 414–422. [CrossRef]
63. Ghosh, S.; Sarkar, B.; Thongmee, S.; Mostafavi, E. Hybrid Antibacterial, Antifungal, and Antiviral Smart Coatings. In *Antiviral and Antimicrobial Smart Coatings*; Kumar, A., Behera, A., Nguyen, T.A., Bilal, M., Gupta, R., Eds.; Elsevier: Amsterdam, The Netherlands, 2023; pp. 431–452.
64. Stevanović, M.; Bajić, Z.J.; Veličković, Z.S.; Karkalić, R.M.; Pecić, L.; Otřísal, P.; Marinković, A.D. Adsorption Performances and Antimicrobial Activity of the Nanosilver Modified Montmorillonite Clay. *Desalin. Water Treat.* **2020**, *187*, 345–369. [CrossRef]

65. Cantero, D.; Pinilla-Peñalver, E.; Romero, A.; Sánchez-Silva, L. Synthesis of Waterborne Polyurethane Aerogels-like Materials via Freeze-Drying: An Innovative Approach. *J. Mater. Sci.* **2023**, *58*, 9087–9102. [CrossRef]
66. Muñoz-Bonilla, A.; Fernández-García, M. Polymeric Materials with Antimicrobial Activity. *Prog. Polym. Sci.* **2012**, *37*, 281–339. [CrossRef]
67. Palenzuela, M.; Valenzuela, L.; Amariei, G.; Vega, J.F.; Mosquera, M.E.G.; Rosal, R. Poly(Glycidyl Methacrylate) Macromolecular Assemblies as Biocompatible Nanocarrier for the Antimicrobial Lysozyme. *Int. J. Pharm.* **2021**, *603*, 120695. [CrossRef]
68. Fazaeli, Y.; Amani, V.; Amini, M.M.; Khavasi, H.R. Bis(tri benzyl ammonium) tetra chloridoaurate(III) chloride. *Acta Cryst. E.* **2010**, *66*, m212. [CrossRef]
69. Groom, C.R.; Bruno, I.J.; Lightfoot, M.P.; Ward, S.C. The Cambridge Structural Database. *Acta Cryst. B* **2016**, *72*, 171–179. [CrossRef]